Microfluid Nanofluid (2009) 7:559–568
DOI 10.1007/s10404-009-0416-7

RESEARCH PAPER

Parameter extraction from BVD electrical model of PZT actuator of micropumps using time-domain measurement technique

Ling-Sheng Jang · Wai-Hong Kan · Ming-Kun Chen · Yao-Min Chou

Received: 21 November 2008 / Accepted: 23 January 2009 / Published online: 17 February 2009

Abstract To minimize the power consumption of the piezoelectric micropumps utilized in the microfluidics field, suitable models are required to enable the optimization of the lead zirconate titanate (PZT) actuator driving circuits. The recent research shows that the electromechanical parameters of piezoelectric materials can be obtained from Butterworth Van-Dyke (BVD) model. The current study presents a novel time-domain measurement technique for extracting the parameters of a BVD electrical model describing a PZT actuator of the micropump excited by a square pulse with a relatively high voltage and low frequency. The validity of the BVD model is evaluated by using MATLAB software to solve the ordinary differential equations of the electrical model and then comparing the numerical results obtained for the current response of the PZT actuator with the experimentally-observed results. The BVD model has been found to be valid for this specific application of piezo actuators. A good agreement is observed between the two sets of result, and thus the validity of the BVD model and the proposed time-domain measurement technique is confirmed.

Keywords PZT actuator · Time-domain measurement · Electrical model · Micropump · Microfluidics

List of symbols

v_1	applied driving voltage
v_2	output voltage
A	the lowest voltage intensity of driving source
N	peak-to-peak voltage of driving source
τ_1	rising time constant of driving source
$i_{C_0}(t)$	current passing through the capacitor branch
$i_s(t)$	current passing through the RLC branch
$i_L(t)$	output current
t_c	the critical time
v_{C_1}	voltage difference across the C_1
ω_d	under-damping resonant frequency
α	damping coefficient
B_1	the cosine coefficient of homogeneous solution of $v_{C_1}(t)$
B_2	the sine coefficient of homogeneous solution of $v_{C_1}(t)$
a	the constant of specific solution of $v_{C_1}(t)$
b	the exponential coefficient of specific solution of $v_{C_1}(t)$

1 Introduction

Rapid advances in the micro-electro-mechanical systems field in recent decades have enabled the development of a wide variety of microfluidic devices ranging from flow sensors, to micro-mixers, cytometers, and so forth, for use in the medical, chemical, pharmaceutical and bio-analysis fields (Nguyen et al. 2002; Bashir 2004). Increasingly, such devices have been integrated on a single substrate to realize multi-functional microchips designated as Lab-on-Chip or micro-total-analysis systems (Bashir 2004; Laser and Santiago 2004).

The performance of such systems relies upon the transportation and manipulation of small, precisely-defined sample volumes within the microfluidic device. As a result, a requirement exists for efficient, miniaturized pumping

L.-S. Jang (✉) · W.-H. Kan · M.-K. Chen · Y.-M. Chou
Department of Electrical Engineering and Center for Micro/Nano Science and Technology, National Cheng Kung University, 1 University Road, Tainan 701, Taiwan
e-mail: lsjang@ee.ncku.edu.tw

schemes capable of implementation at the chip-level. This requirement is commonly satisfied using some form of piezoelectrically-actuated micropump. Various types of piezoelectric material exist, including barium titanate, bismuth titanate, lead zinc titanate (PZT), niobium-lead zirconate titanate (PNZT), and so forth. Of these materials, PZT is one of the most commonly employed for actuation purposes in the microfluidics field due to its high driving force, broad actuation range, wide operational frequency range, and low power consumption (Olsson et al. 1997; Setter et al. 2006; Muralt 2000). To support the requirement for portable micropump systems such as attaining sufficient flow rates and pressure, a low-order model was proposed and used to optimize the resonant behavior of the micropump with fix-valve by adjusting proper geometric or material parameters (Morris and Forster 2003). However, the power consumption is also a critical issue for practical applications. Therefore, it is essential to optimize the driving circuits of these PZT actuators in such a way as to minimize their power consumption (Jang et al. 2007).

The vibration phenomena in piezoelectric systems are commonly analyzed using electro-mechanical equivalent circuits or the Butterworth Van-Dyke (BVD) model. The four-element BVD model used to describe crystal resonators involves two parallel branches including the parallel capacitance C_0 and RLC branch composed of resistance R_1,capacitance C_1 and inductance L_1 (Valimaki et al. 1997; Naik et al. 1998). The model is predicted to match the theoretically derived electrical behavior of the fundamental-mode resonance and adopted by the IEEE Standard on piezoelectricity (Standards Committee of the IEEE Ultrasonics, Ferroelectrics, and Frequency Control Society 1987). One branch consisting of only the capacitance C_0 represents the fixed dielectric capacitance of the resonator. The other RLC branch represents the motional behavior of piezoelectrics. Resonance characteristics such as the resonant frequency f_s and quality factor Q can be determined in the RLC branch. The literature contains many investigations into the application of equivalent circuits for the simulation, design and optimization of piezoelectric transducers (Mason 1948; Redwood 1961; Kirmholtz et al. 1970). These equivalent circuits require the mechanical parameters of transducers. In the study of optimizing the driving circuits of the PZT actuators used in micropumps, the BVD model is suitable because it represents the electrical response of piezoelectric and does not require the mechanical parameters of transducers. However, the BVD model is valid only when the model parameters are constant and independent of the frequency, which occurs only for a narrow range of frequencies near the resonance frequency (Standards Committee of the IEEE Ultrasonics, Ferroelectrics, and Frequency Control Society 1987). The PZT actuators used in reciprocating-type displacement micropumps are generally excited using a square waveform with a relatively high voltage (50–450 V) and low frequency (0.1 Hz–5 kHz; Laser and Santiago 2004; Husband 2004). Therefore, the operating conditions are located far from this resonance frequency range. Moreover, piezoelectric materials exhibit a nonlinear polarization-electrical (P-E) field relationship under high field strengths. As a result, piezoelectrics exhibit a nonlinear dielectric characteristic (Hall 2001). Consequently, the method used to extract the parameters of the BVD model must be modified in some way to ensure the reliability of the extracted results.

The parameters in a typical BVD model are generally extracted using impedance or network analyzers. Alternative techniques have also been prescribed by the Institute of Electrical and Electronics Engineers (Standards Committee of the IEEE Ultrasonics, Ferroelectrics, and Frequency Control Society 1978) and the International Electrotechnical Commission (IEC 1986), respectively. However, their measurement circuits are very complex. In addition, Arnau et al. (Arnau et al. 2000) presented a method of determining BVD parameters of a quartz crystal microbalance in fluid media using a continuous motional series resonant frequency monitoring circuit. Furthermore, the decay scheme used in AT-cut quartz crystal microbalance sensors (Rodahl and Kasemo 1996a, b) can detect all four parameters in a time-domain with two different circuits (Rodahl et al. 1996). However, both methods are inapplicable to the analysis of the PZT actuators used in microfluidic micropumps since the two driving signals are sinusoidal rather than square and have a low rather than high voltage level. Therefore, a requirement exists for simpler methods for extracting the parameters of BVD actuator model.

To resolve the limitations of the schemes described above, the current study presents a novel time-domain measurement approach for extracting the parameters of the BVD model of a PZT actuator driven by a high-voltage, low-frequency square waveform. The validity of the proposed approach is evaluated by using MATLAB software to solve the ordinary differential equations (ODEs) of the electrical model and confirmed by comparing the results obtained for the current response of the PZT actuator with the corresponding experimental results.

2 Methods and results of physical experiments

2.1 Micropump fabrication

Figure 1 presents a schematic illustration of the micropump fabricated in the current study. As shown, the pump comprises three major components, namely a Pyrex glass substrate, a silicon membrane and a commercially-available bulk PZT chip (T107-H4E-602; Piezo Systems, Inc.; Jang

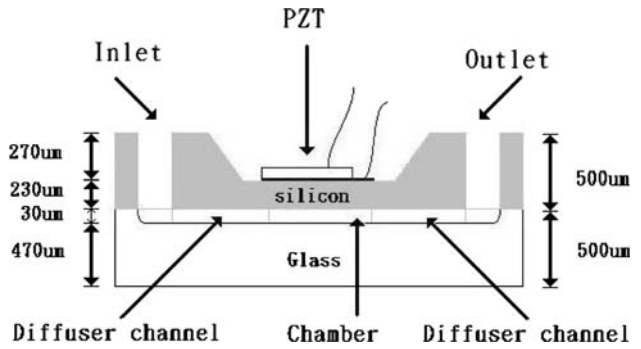

Fig. 1 Schematic diagram showing major components of micropump and corresponding dimensions

et al. 2005). The fabrication process commenced by using an e-beam evaporation process to deposit chromium (Cr) and gold (Au) films on the Pyrex substrate. The Cr/Au film was then patterned using standard photolithography techniques. Finally, the diffuser channel and pump chamber [measuring 6 mm × 30 μm (diameter × depth)] were etched using a solution of 49% hydrofluoric acid. The silicon membrane was fabricated by using a low-pressure chemical vapor deposition technique to coat both sides of a (100) silicon wafer with a silicon nitride layer with a thickness of 200 nm. A square opening was then formed in the silicon nitride layer by using a reactive ion etching (RIE) technique followed by an etching process performed using a 45% potassium hydroxide (KOH) etchant at a temperature of 80°C. Finally, the two-sided nitride protection layers were stripped using RIE. Having etched the silicon wafer to form the actuation membrane with a thickness of 230 μm, a drill with a diamond bit was used to drill two holes in either end of the wafer to form the inlet and outlet channels of the micropump, respectively. Finally, the silicon wafer and Pyrex substrate were carefully aligned and bonded anodically using a voltage of 1,000 V at a temperature of 475°C. The micropump was completed by attaching a PZT chip measuring 6 mm × 6 mm to the silicon membrane using silver epoxy, and connecting inlet and outlet tubes and two electrical connecters to the pump body using epoxy glue.

2.2 Experimental setup

Figure 2a presents the time-domain measurement test circuit used in the present study to determine the parameters of the actuator model. The square pulse input signal (v_1) was produced using a function generator (FG 503; Motech). This signal was amplified by a PCB790 power amplifier (Piezotronics) and then supplied to the device under test, i.e. the bulk PZT chip, through one of the electrical connectors. A 1-kΩ resistor was then connected between the second connector and the ground. During the experiments, the input (v_1) and output (v_2) signals of the bulk PZT chip were recorded using a TDS2014 digital oscilloscope (Tektronix).

In practical applications, the micropump is operated without a resistor between the actuator and the ground. However, in the present experiments, this resistor is required in order to enable the electrical response of the PZT to be evaluated. Note that in choosing a suitable resistor, a value of 1 kΩ was specifically chosen since this value is significantly lower than the mean impedance of the moving PZT actuator and therefore has no effect on the PZT response.

The test circuit shown in Fig. 2b is simpler than existing circuits used to determine the PZT actuator model. Moreover, the circuit provides a far cheaper means of extracting the actuator parameters than traditional network analyzers.

2.3 Experimental results

Utilizing the circuit shown in Fig. 2b, the driving voltage, v_1, and output voltage, v_2, were measured using the digital oscilloscope under the following conditions:

(1) A square wave driving voltage (v_1) with a magnitude of −5 V to +5 V, a frequency of 100 Hz, and a duty cycle of 50%.
(2) A power amplifier gain setting of ×10.

Figure 3a presents the corresponding experimental results.

3 Analytical approach

3.1 General observations on experimental data

To analyze the experimental data shown in Fig. 3a, the output voltage response must be changed into the equivalent current response. The output current, $i_L(t)$, is given by $i_L(t) = v_2(t)/R_L$, and is equal to the sum of the currents passing through the capacitor branch $[i_{C_0}(t)]$ and the RLC branch $[i_s(t)]$, respectively, of the BVD actuator model shown in Fig. 2b. The RLC branch comprising R_1, L_1 and C_1 is the well-known under-damping current response model of conventional electric circuit theory. According to the experimental results of Fig. 3b, it represents the procedure of charging the capacitor (PZT ceramics) through the resistor R_L. As a result, the driving voltage v_1 has the form of exponential response with a RC time constant τ_1. When the voltage v_1 reaches 99.95% of its maximum value (at the time t_c over than $5\tau_1$), the source can be regarded as reaching the steady state, $v_1(t) \approx 50$ V (staying within a stated plus-and-minus tolerance band around its final value) (Doebelin 1990). Meanwhile, the corresponding current passing through the PZT ceramics is relatively low and decaying as shown in Fig. 3b. It means that the charges accumulation on

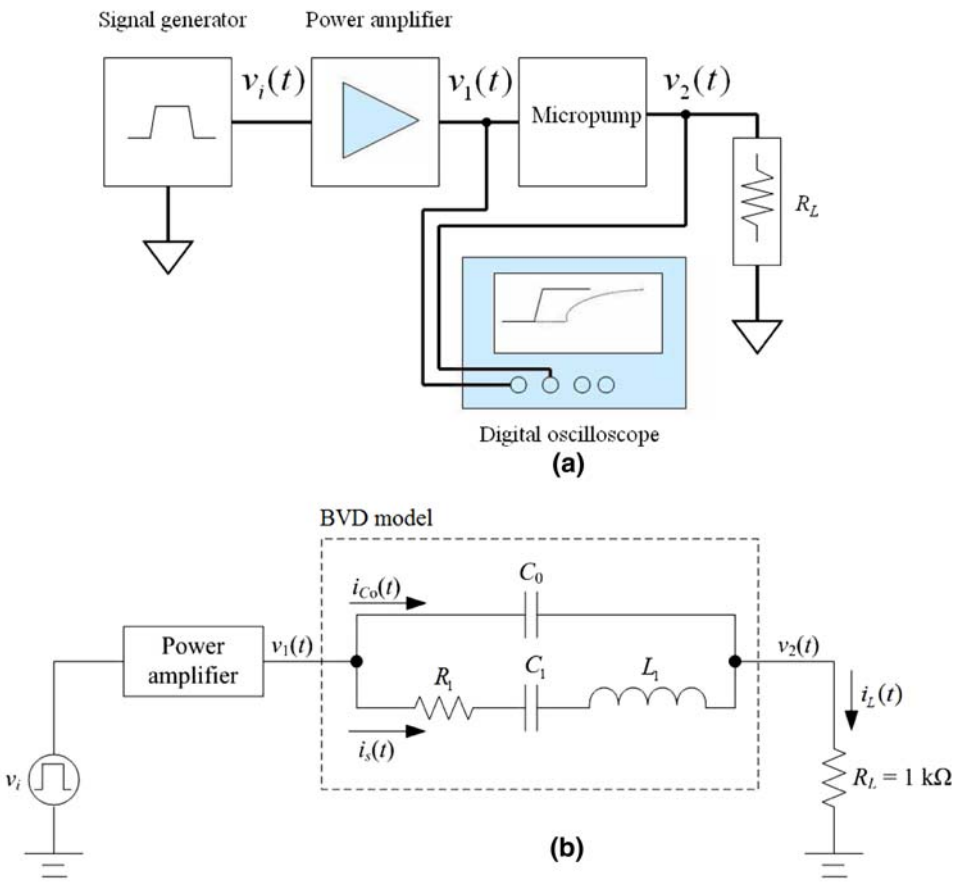

Fig. 2 **a** The experimental setup of measurement part **b** BVD actuator model added in place of micropump in time-domain testing circuit. Note that $i_L(t) = i_{C_0}(t) + i_s(t)$

the parallel plate of the PZT ceramics is decaying and the volume of PZT tends to be stable. We define the instant as the critical time t_c for distinguishing physical motion of PZT actuator. At the time $t < t_c$, the mechanical motion of the PZT actuator which is to significantly deform the diaphragm dominates the overall response. In addition, at the time $t > t_c$, the PZT actuator has a tendency towards steady-state. Thus, the current through the PZT actuator has the under-damping phenomenon. For purpose of simplifying the calculation, the current response, $i_L(t)$, can be partitioned into two regions, namely $i_{C_0}(t)$-dominated at times (t) less than a certain critical time t_c, and $i_s(t)$-dominated at times $t > t_c$. The exponential responses of the PZT actuator for $t < t_c$ and $t > t_c$, respectively, are discussed in the sections which follow.

3.2 Exponential response of PZT actuator for $t < t_c$

This section derives the mathematical expression for $i_{C_0}(t)$ for $t < t_c$. From a modeling perspective, the RLC branch in the BVD model can be removed such that the test circuit reduces to the series RC circuit. Applying Kirchhoff's Voltage Law (KVL) to this simplified circuit, it can be shown that

$$A + N\left(1 - \mathrm{e}^{-t/\tau_1}\right) = \frac{1}{C_0}\int_0^t i_{C_0}(t)\mathrm{d}t + i_{C_0}(t)R_L \tag{1}$$

where C_0 is the capacitance of the PZT ceramics, A is the lowest voltage intensity of the amplified square pulse signal (v_1), N is the peak-to-peak voltage, and τ_1 is the rising time constant of v_1. Equation 1 can be rearranged in the form

$$\frac{\mathrm{d}i_{C_0}(t)}{\mathrm{d}t} + \frac{1}{R_L C_0} i_{C_0}(t) = \frac{N}{R_L \tau_1}\mathrm{e}^{-t/\tau_1} \tag{2}$$

Equation 2 is a first-order ODE. The term $i_{C_0}(t)$ in Eq. 2 can be solved by applying the integrating factor $\mathrm{e}^{t/R_L C_0}$, i.e.

$$i_{C_0}(t) = \frac{N/R_L}{(\tau_1/R_L C_0) - 1} \times \left(\mathrm{e}^{-t/\tau_1} + K\mathrm{e}^{-t/R_L C_0}\right) \tag{3}$$

where K is an arbitrary constant and substituting the initial condition $i_{C_0}(0) = 0$ into Eq. 3 gives $K = -1$ and

$$i_{C_0}(t) = \frac{N/R_L}{(\tau_1/R_L C_0) - 1} \times \left(\mathrm{e}^{-t/\tau_1} - \mathrm{e}^{-t/R_L C_0}\right) \tag{4}$$

As shown in Eq. 4, the value of $i_{C_0}(t)$ is determined by N, τ_1, R_L and C_0. In Eq. 4, C_0 is the only unknown and can

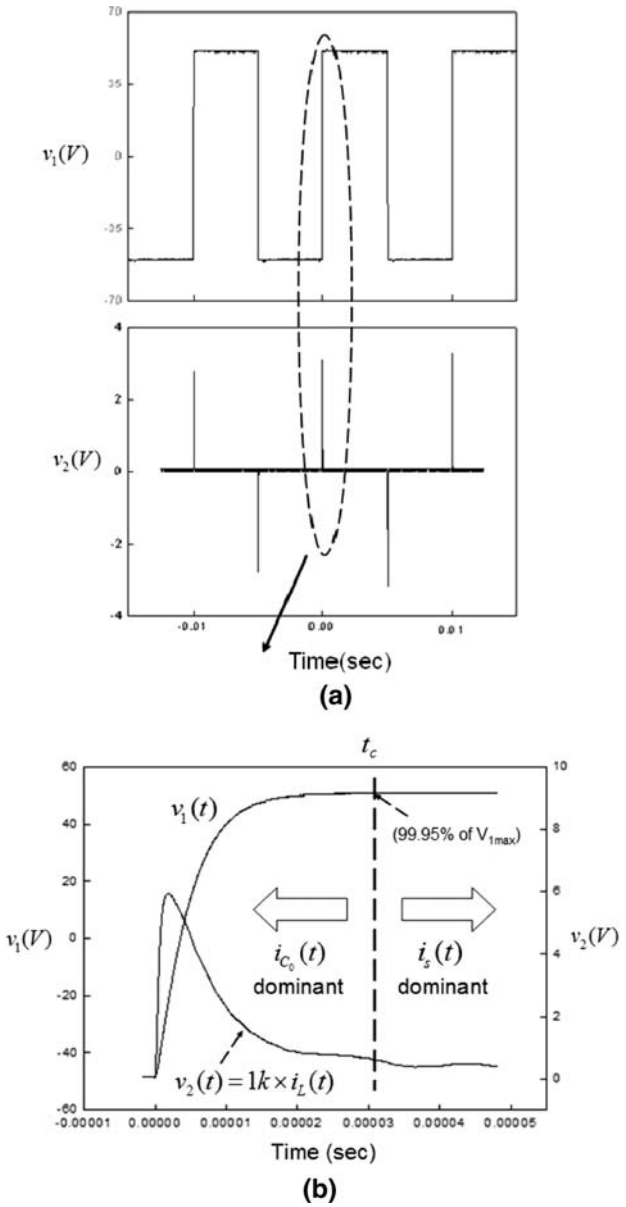

Fig. 3 **a** Experimental results obtained for input and output signals of PZT actuator **b** partitioning of experimental data for $v_2(t)$ presented into two sections, namely $i_{C_0}(t)$-dominated and $i_s(t)$-dominated

therefore be easily obtained by performing MATLAB simulations using the experimental data presented in Fig. 3.

3.3 Solving for C_0

$C_0(v_1)$ can be determined from Eq. 4 using the experimental data obtained for the output voltage response $v_2(t)$. In Eq. 4, $C_0(v_1)$ is the only unknown since $i_{C_0}(t)$, v_1, τ_1 and t can all be derived directly from the experimental data and the value of R_L is known in the test circuit. The time constant (τ_1) of the PZT input signal can be found by nonlinear least-squares curve fitting $v_1(t)$ using OriginPro 7.0 software. Figure 4 shows the fitted curve of v_1. The absolutely maximum deviation between the v_1 and the fitted curve is up to about 5 V. The error resulting from the dynamic RC time constant is because of the nonlinear property of piezoelectric ceramics under relatively high electric intensity. Obtaining the solution for $C_0(v_1)$ involves solving a nonlinear one-variable equation and thus Eq. 4 is easily solved using the MATLAB built-in solve function. Figure 5 illustrates that C_0 varies over the range 0.5–5 nF as the driving voltage is increased from −50 V to +50 V. According to Fig. 5, C_0 increases slowly and a sharp upturn happens when the driving voltage v_1 almost reaches its maximum value. The following discussion is our hypothesis regarding this phenomenon. We consider the piezoelectric ceramics as an ideal parallel-plate capacitor whose capacitance can be represented using the Eq. 5,

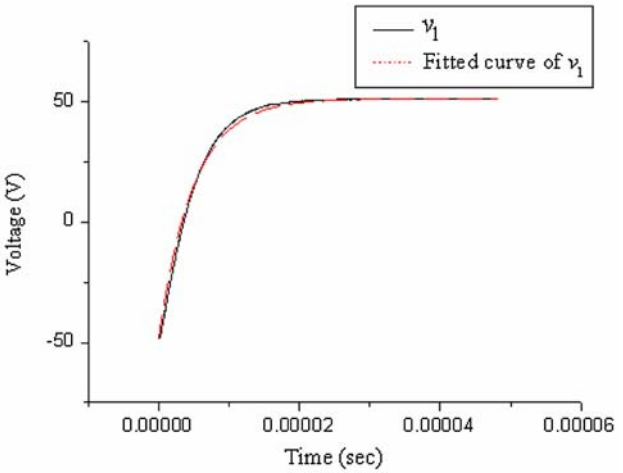

Fig. 4 Comparison of the driving voltage v_1 indicated as the *solid line* and the fitted curve of v_1 marked as the *dotted line*

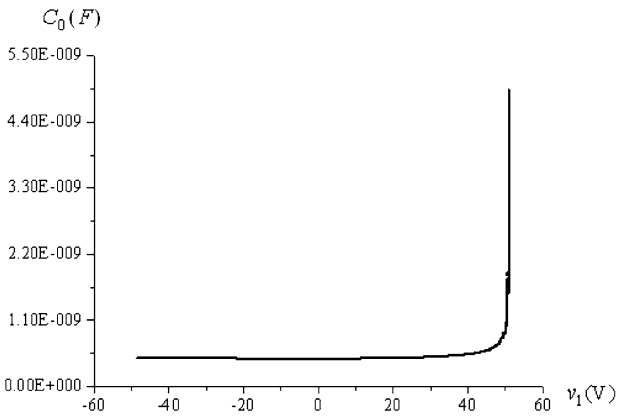

Fig. 5 Variation of C_0 with driving voltage

$$C_0 = \varepsilon \frac{A}{d} \tag{5}$$

where C_0, A and d denote the capacitance, surface area and thickness of the piezoelectric ceramics, respectively. Prior investigation into the nonlinear properties of piezoelectric ceramics showed that the dielectric constant ε of a piezoelectric material increases as the intensity of the applied electric field increases (Hall 2001). Based on Eq. 5, the capacitance C_0 is proportional to the dielectric constant ε and reversely proportional to the thickness d of PZT material with assumption of the constant surface area A. As aforementioned, the critical time t_c is defined as the time where the driving voltage reaches 99.95% of its maximum. At the time $t < t_c$, the mechanical motion of the PZT actuator dominates the overall response. The dielectric constant ε and thickness d increase as the driving voltage increases. Therefore, the combination of these two effects makes C_0 increase slowly. At time $t > t_c$, the motion of the PZT actuator finishes and the under-damping phenomenon dominates the response of the PZT actuator. At this stage, the thickness d of the PZT actuator can be considered as constant. However, the dielectric constant ε still increases as the driving voltage increases. Therefore, the sharp upturn of the C_0 curve happens due to the effect of the dielectric constant ε when driving voltage v_1 is reaching the steady state.

3.4 Exponential response of PZT for $t > t_c$

As discussed in Sect. 3.1, $i_s(t) \approx i_L(t)$ when $t > t_c$. This section derives the basic equations for parameters R_1, L_1 and C_1 in the RLC branch of the BVD actuator model. From a modeling perspective, the basic equations for the parameters in the RLC branch of the BVD model can be obtained by regarding the C_0 branch as an open circuit such that the test circuit can be simplified. The procedure of algebraic operation and basic RLC circuit analysis math is shown in Appendix. The general solution of RLC circuit has five undetermined coefficients a, b, B_1, B_2 and α which are given by the following equation:

$$v_{C_1}(t) = (B_1 \cos \omega_d t + B_2 \sin \omega_d t)e^{-\alpha t} + a + be^{-t/\tau_1} \tag{6}$$

where α is the damping coefficient and ω_d is the damped angular frequency. The solution procedure for Eq. 6 commences by deriving the values of a and b, as discussed in Sect. 3.4.1. Thereafter, these values are used to determine the values of B_1 and B_2 subject to the assumed initial condition of $v_{C_1}(0) = A$ (see Sect. 3.4.2). The value of α is obtained by choosing the experimental data obtained for $v_2(t)$ corresponding to an input voltage of $v_1(t) \approx A + N$, $t > t_c$, in order to simplify the calculation, and applying the periodic characteristic of an under-damped response, as described in Sect. 3.4.3. Finally, the relationship between R_1 and C_1 is established (see Sect. 3.4.4).

3.4.1 Determining a and b

Substituting v_p, v'_p and v''_p into Eq. 40, a and b can be acquired by comparing coefficients, i.e.

$$a = A + N \tag{7}$$

and

$$b = \frac{-\frac{N}{L_1 C_1}}{\frac{1}{\tau_1^2} - \frac{R'}{L_1 \tau_1} + \frac{1}{L_1 C_1}} \tag{8}$$

Using these formulations for a and b, and applying Eq. 37, Eq. 36 can be rewritten as

$$v_{C_1}(t) = (B_1 \cos \omega_d t + B_2 \sin \omega_d t)e^{-\alpha t} + (A + N) - \frac{\frac{N}{L_1 C_1}}{\frac{1}{\tau_1^2} - \frac{R'}{L_1 \tau_1} + \frac{1}{L_1 C_1}} e^{-t/\tau_1} \tag{9}$$

3.4.2 Determining B_1 and B_2

Substituting the initial condition $v_{C_1}(0) = A$ into Eq. 9 yields

$$v_{C_1}(0) = B_1 + (A + N) - \frac{\frac{N}{L_1 C_1}}{\frac{1}{\tau_1^2} - \frac{R'}{L_1 \tau_1} + \frac{1}{L_1 C_1}} = A \tag{10}$$

or

$$B_1 = \frac{\tau_1 R' C_1 - L_1 C_1}{\tau_1^2 - \tau_1 R' C_1 + L_1 C_1} N \tag{11}$$

To extract B_2, it is first necessary to analyze $v'_{C_1}(t)$. The differential of Eq. 9 is given by

$$v'_{C_1}(t) = -\alpha(B_1 \cos \omega_d t + B_2 \sin \omega_d t)e^{-\alpha t} + \omega_d(-B_1 \sin \omega_d t + B_2 \cos \omega_d t)e^{-\alpha t} + \frac{N\tau_1}{\tau_1^2 - \tau_1 R_1 C_1 + L_1 C_1} e^{-t/\tau_1} \tag{12}$$

Substituting the differential of the initial condition $v'_{C_1}(0) = 0$ into Eq. 12 gives

$$\frac{dv_{C_1}(0)}{dt} = -\alpha B_1 + B_2 \omega_d + \frac{N\tau_1}{\tau_1^2 - \tau_1 R' C_1 + L_1 C_1} = 0 \tag{13}$$

or

$$B_2 = \frac{\tau_1 R' C_1 \alpha - L_1 C_1 \alpha - \tau_1}{\tau_1^2 - \tau_1 R' C_1 + L_1 C_1} \times \frac{N}{\omega_d} \tag{14}$$

3.4.3 Determining α

This section commences by showing that a and b can actually be ignored when extracting the RLC branch parameters of the BVD model. A simple expression for α is

then derived based upon the periodicity of an under-damped response.

Ignoring a and b The experimental data of $v_2(t)$ is obtained for the case in which $v_1(t) \approx A + N$, $t > t_c$, and b in Eq. 6 can be ignored since $v_1(t) \approx A + N\left(1 - e^{-t/\tau_1}\right)$. Hence, Eq. 6 can be simplified to the following form:

$$v_{C_1}(t) = (B_1 \cos \omega_d t + B_2 \sin \omega_d t)e^{-\alpha t} + a \tag{15}$$

Since the aim of the current study is to analyze the current response of a micropump and $i_s(t) = C_1(dv_{C_1}(t)/dt)$, the current passing through RLC branch can be obtained as:

$$\begin{aligned} i_s(t) = &-C_1\alpha(B_1 \cos \omega_d t + B_2 \sin \omega_d t)e^{-\alpha t} \\ &+ C_1\omega_d(-B_1 \sin \omega_d t + B_2 \cos \omega_d t)e^{-\alpha t} \end{aligned} \tag{16}$$

Note that in Eq. 16, the constant a in Eq. 15 no longer appears. Equation 16 can be rearranged in the form

$$i_s(t) = C_1 e^{-\alpha t}[(B_2\omega_d - B_1\alpha)\cos \omega_d t - (B_2\alpha + B_1\omega_d)\sin \omega_d t] \tag{17}$$

Ignoring B_1 and B_2 and determining α Due to the periodicity of an under-damped response of the PZT actuator, some eigenvalues can be identified in the current response $v_2(t)$. Figure 6 indicates the positions of these eigenvalues (t_{c1}, t_z and t_{c2}). Note that in this figure, t_{c1} and t_{c2} denote the two adjacent local maximum times in $v_2(t)$ and t_z is the time at which $i_s(t_z) = 0$. The corresponding currents at times t_{c1}, t_{c2} and t_z are denoted as $i_s(t_{c1})$, $i_s(t_{c2})$ and $i_s(t_z)$, respectively. The eigenvalues in $v_2(t)$ are used to calculate R_1, L_1 and C_1 as follows.

First, substituting t_{c1} and t_{c2} into Eq. 17 yields the corresponding currents $i_s(t_{c1})$ and $i_s(t_{c2})$, i.e.

$$\begin{aligned} i_s(t_{c1}) = C_1 e^{-\alpha t_{c1}} &\left[\left(B_2\omega_d - B_1\alpha\right)\cos \omega_d t_{c1}\right. \\ &\left.-\left(B_2\alpha + B_1\omega_d\right)\sin \omega_d t_{c1}\right] \end{aligned} \tag{18}$$

and

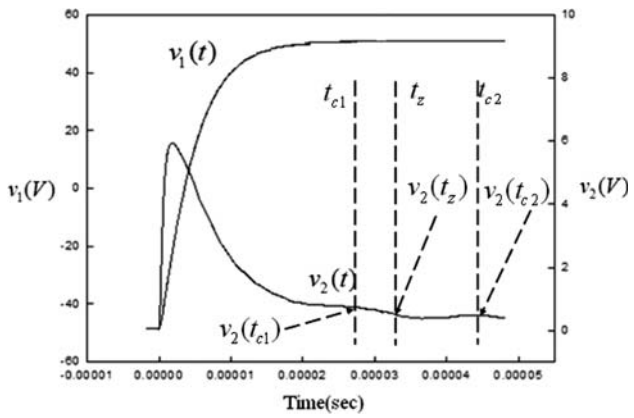

Fig. 6 Specific times for determining R_1, L_1 and C_1, where $i_s(t_x) = v_2(t_x)/R_L$

$$\begin{aligned} i_s(t_{c2}) = C_1 e^{-\alpha t_{c2}} &\left[\left(B_2\omega_d - B_1\alpha\right)\cos \omega_d t_{c2}\right. \\ &\left.-\left(B_2\alpha + B_1\omega_d\right)\sin \omega_d t_{c2}\right] \end{aligned} \tag{19}$$

where $B_2\omega_d - B_1\alpha$ and $B_2\alpha + B_1\omega_d$ are constants. Due to the periodic characteristic of the under-damped response, $\cos \omega_d t_{c1}$ equals $\cos \omega_d t_{c2}$ and $\sin \omega_d t_{c1}$ equals $\sin \omega_d t_{c2}$. Therefore, dividing Eq. 18 by Eq. 19 yields

$$\frac{i_s(t_{c1})}{i_s(t_{c2})} = \frac{e^{-\alpha t_{c1}}}{e^{-\alpha t_{c2}}} \tag{20}$$

or

$$\alpha = \frac{1}{T}\ln\left|\frac{i_s(t_{c1})}{i_s(t_{c2})}\right| \tag{21}$$

with

$$T = \frac{2\pi}{\omega_d} = t_{c2} - t_{c1} \tag{22}$$

where T is the time difference between two adjacent local maximum time and ω_d is derived from the experimental data. Equation 21 shows that α has a simple formulation and is easily found from the experimental data.

3.4.4 *Determining correlation between R' and C_1*

If a time t_z exists, let $i_s(t_z) = 0$ (Fig. 5), Eq. 17 can be then modified to the following form:

$$\begin{aligned} i_s(t_z) = C_1 e^{-\alpha t_z} &\left[\left(B_2\omega_d - B_1\alpha\right)\cos \omega_d t_z\right. \\ &\left.-\left(B_2\alpha + B_1\omega_d\right)\sin \omega_d t_z\right] = 0 \end{aligned} \tag{23}$$

or

$$\tan \omega_d t_z = \frac{B_2\omega_d - B_1\alpha}{B_2\alpha + B_1\omega_d} \tag{24}$$

Rewriting Eq. 24 in terms of the formulations given for B_1 and B_2 in Eqs. 11 and 14, respectively, it can be shown that

$$\tan \omega_d t_z = \frac{-\tau_1}{(\tau_1 R' C_1 - L_1 C_1)\left(\frac{\alpha^2+\omega_d^2}{\omega_d}\right) - \frac{\tau_1\alpha}{\omega_d}} \tag{25}$$

or

$$R'C_1 = \frac{(1 + \alpha\tau_1)\tan \omega_d t_z - \omega_d \tau_1}{\tau_1(\alpha^2 + \omega_d^2)\tan \omega_d t_z} \tag{26}$$

where τ_1, ω_d, α and t_z are now known. Thus, the relationship between R' and C_1 is identified.

4 Applications of analytical approach to experiment data

4.1 Determining values of R', L_1 and C_1

As shown in the previous section, α and ω_d can be obtained from Eqs. 21 and 22, respectively. Furthermore, rearranging Eqs. 38 and 39 gives

Table 1 The overall parameters in BVD model

Parameter	Value
C_0	0.5–5 nF
$R(R' - R_L)$	5.76 kΩ
L_1	951.2 mH
C_1	7.8 pF

$$R' = 2\alpha L_1 \tag{27}$$

and

$$L_1 = \frac{1}{C_1(\omega_d^2 + \alpha^2)} \tag{28}$$

Under the assumption that R', L_1 and C_1 remain constant during the PZT actuation process, their values can be obtained by using Eqs. 26, 27 and 28 with the experimental data presented in Fig. 3. The four parameters of BVD model are therefore obtained using the method described above. Table 1 indicates the overall parameters of the PZT micropump model used in the current study.

4.2 Verification of BVD model

In this section, the BVD model is analyzed using the conventional electric circuit mesh method. The ODEs identified using the mesh method are solved by MATLAB (Ajitsaria et al. 2007). The validity of the BVD model is then verified by comparing the simulations results obtained for the current response of the PZT actuator with the experimental results. In Fig. 7, the equation for mesh 1 is given by

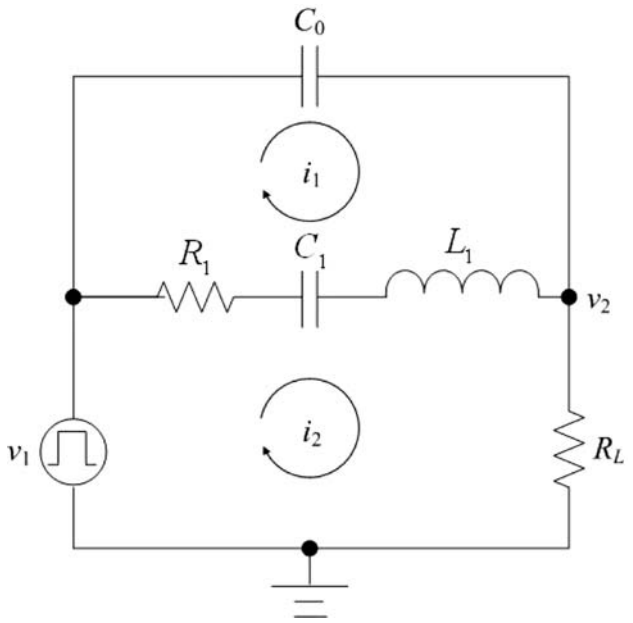

Fig. 7 Analyzing test circuit using mesh method, where v_1 is the same as that shown in Fig. 3a

$$\frac{d(v_1 - v_2)}{dt} = \frac{i_1}{C_0} \tag{29}$$

and becomes

$$\frac{di_2}{dt} + \frac{i_2}{R_L C_0} + \left(\frac{y}{C_0} - \frac{dv_1}{dt}\right)\frac{1}{R_L} = 0 \tag{30}$$

where

$$y = i_1 - i_2 \tag{31}$$

Similarly, the equation for mesh 2 has the form

$$(i_2 - i_1)R_1 + L_1\frac{d(i_2 - i_1)}{dt} + v_{C_1} + i_2 R_L - v_1 = 0 \tag{32}$$

or

$$\frac{d^2y}{dt^2} + \frac{R_1}{L_1}\frac{dy}{dt} + \frac{y}{L_1 C_1} - \frac{R_L}{L_1}\frac{di_2}{dt} + \frac{1}{L_1}\frac{dv_1}{dt} = 0 \tag{33}$$

Equations 30 and 33 contain two independent variables, namely y and i_2. The resulting differential-algebraic problem can be solved using the ODE function in MATLAB. Figure 8 shows the simulation results obtained for the current response of the PZT actuator based on the BVD model with C_0, R_1, L_1 and C_1 derived in current study. The maximum and minimum errors are 21.9 and 14.7%, respectively. The mean square error between the simulation and experiment results is 2.32E-7. The maximum error up to 21.9% may result from the inaccurate fitting result of v_1 which is used to solve parameter C_0 in Eq. 4. As shown in Fig. 4, the fitted curve is less than the practical input driving voltage from $t = 5.9 \times 10^{-6}$ s to $t = 3.3 \times 10^{-5}$ s. The maximum deviation is up to 5 V and makes the solution of parameter C_0 smaller than the actual capacitance of PZT actuator. Therefore, the peak current of the simulation is less than that of the experiment. In addition, the other thing needed to be noticed in the damped current is the shift in phase. Since the calculated angular frequency is determined by measuring the interval of the eigenvalues t_{c1} and t_{c2}, the calculated and observed damped angular frequencies are the same. The difference in the damped current between the calculated and observed data may result from that the BVD model cannot totally interpret our PZT system. According to Fig. 8, the solid line and dotted line indicate the calculated current of $i_L(t)$ and $i_s(t)$, respectively and the experiment data is denoted as dashed line. By comparing the dashed and dotted lines, we can see that the under-damping component of the current is not in phase. The shift of phase may result from the definition of initial condition used in mathematical method to calculate the current passing through PZT ceramics. As shown in the Fig. 8, the calculated under-damping current (dotted line) occurs at $t = 0$, while in practice the under-damping phenomenon of PZT material may not appear at $t = 0$ and hence has a shift in phase. Generally, it is observed that the

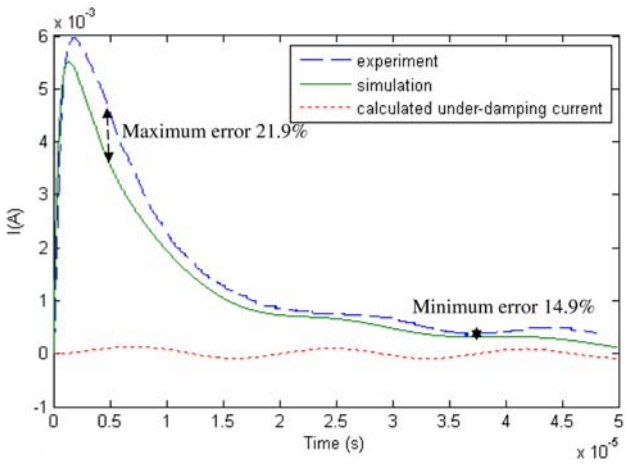

Fig. 8 Comparison of simulation and experimental results for variation of PZT current response over time at a square-wave driving voltage v_1 with peak-to-peak amplitude of 100 V and operation frequency of 100 Hz

trend of simulation results are in good agreement with that of the experimentally observed current response, and thus the validity of the extracted BVD model is confirmed.

5 Conclusions

This study has employed a time-domain measurement technique implemented using MATLAB software to extract the parameters of a BVD model describing the current response of a PZT actuator excited by a high-voltage, low-frequency square wave driving signal. The good agreement observed between the trend of the simulated current response and the experimental response using MATLAB software confirms the validity of the proposed modeling approach. The current response at the output of the PZT actuator determines the power consumption of the actuated PZT. To achieve the goal of portable micropumps, it is desirable to constrain this current response through the use of appropriate circuitry or by changing the input conditions. In practice, the power consumption of the PZT actuator can be reduced in a number of different ways, e.g. by increasing the input time constant, reducing the input voltage intensity, and so forth. Overall, the results presented in this study indicate that the proposed time-domain measurement method represents a viable technique for evaluating different design strategies when seeking to optimize the driving circuits of PZT actuators and is therefore of considerable benefit in improving the micropump driving electronics.

Acknowledgments This study was supported by the National Science Council of Taiwan under Grant No. NSC 95-2622-E-006-039-CC3. The authors would like to thank the Center for Micro/Nano Science and Technology and the National Nano Device Laboratories, both of Tainan, Taiwan, for their provision of technical support and the access provided to major items of equipment. Additionally, the authors wish to make it known that the current study made use of Shared Facilities supported by the Program of Top 100 Universities Advancement sponsored by the Ministry of Education, Taiwan.

Appendix: Procedure of solving the RLC branch

Applying the KVL to this simplified circuit, the RLC series circuit, it can be shown that

$$i_s R' + v_{C_1} + L_1 \frac{\mathrm{d}i_s}{\mathrm{d}t} = A + N(1 - \mathrm{e}^{-t/\tau_1}) \tag{34}$$

where $R' = R_1 + R_L$, v_{C_1} is the voltage difference across C_1, and A, N and τ_1 represent the minimum voltage intensity, the peak-to-peak voltage and the rising time constant, respectively, of the amplified square pulse voltage (v_1). Since $i_s = C_1(\mathrm{d}v_{C_1}/\mathrm{d}t)$, and given the assumption of an initial condition $v_{C_1}(0) = A$, Eq. 34 can be rewritten in the form of the following second-order differential equation:

$$\frac{\mathrm{d}^2 v_{C_1}}{\mathrm{d}t^2} + \frac{R'}{L_1}\frac{\mathrm{d}v_{C_1}}{\mathrm{d}t} + \frac{v_{C_1}}{L_1 C_1} = \frac{A + N(1 - \mathrm{e}^{-t/\tau_1})}{L_1 C_1} \tag{35}$$

in which the general solution of v_{C_1} has the form

$$v_{C_1}(t) = v_{\mathrm{h}}(t) + v_{\mathrm{p}}(t) \tag{36}$$

The homogeneous term in Eq. 34 is given by

$$v_{\mathrm{h}}(t) = (B_1 \cos \omega_{\mathrm{d}} t + B_2 \sin \omega_{\mathrm{d}} t)\mathrm{e}^{-\alpha t} \tag{37}$$

with

$$\alpha = \frac{R'}{2L_1} \tag{38}$$

and

$$\omega_{\mathrm{d}} = \sqrt{\frac{1}{L_1 C_1} - \alpha^2} = \frac{2\pi}{T} \tag{39}$$

where α is the damping coefficient, ω_{d} is the damped angular frequency and T is the damped period. Note that the value of ω_{d} can be easily determined from the experimental data and is discussed in Sect. 3.2. However, α, B_1 and B_2 are all unknowns with constant values.

The particular term in Eq. 34 has the form

$$v_{\mathrm{p}}(t) = a + b\mathrm{e}^{-t/\tau_1} \tag{40}$$

where a and b are constants and unknown.

References

Ajitsaria J, Choe SY, Shen D, Kim DJ (2007) Modeling and analysis of a bimorph piezoelectric cantilever beam for voltage generation. Smart Mater Struct 16:447–454

Arnau A, Sogorb T, Jiménez Y (2000) A continuous motional series resonant frequency monitoring circuit and a new method of determining Butterworth-Van Dyke parameters of a quartz crystal microbalance in fluid media. Rev Sci Instrum 71:2563–2571

Bashir R (2004) BioMEMS: state-of-the-art in detection, opportunities and prospects. Adv Drug Deliv Rev 56:1565–1586

Doebelin EO (1990) Measurement systems application and design, 4th edn edn. McGraw-Hill, New York, pp 109–110

Hall DA (2001) Review nonlinearity in piezoelectric ceramics. J Mater Sci 36:4575–4601

Husband B (2004) Investigation for the operation of an integrated peristaltic micropump. J Micromech Microeng 14:S64–S69

IEC (1986) Measurement of quartz crystal unit parameters by zero phase technique in a pi-network (Part 1). International electrotechnical commission-IEC standard, publication 44–1, Geneva

Jang LS, Chao SH, Holl MR, Meldrum DR (2005) Microfluidic circulatory flows induced by resonant vibration of diaphragms. Sensor Actuator A 122:141–148

Jang LS, Li YJ, Lin SJ, Hsu YC, Yao WS, Tsai MC, Hou CC (2007) A stand-alone peristaltic micropump based on piezoelectric actuation. Biomed Microdevices 9:185–194

Kirmholtz R, Leedom DA, Mathaei GL (1970) New equivalent circuit for elementary piezoelectric transducers. Electron Lett 6:398–399

Laser DJ, Santiago JG (2004) A review of micropumps. J Micromech Microeng 14:R35–R64

Mason WP (1948) Electromechanical transducers and wave filters. D Van Nostrand, New York

Morris CJ, Forster FK (2003) Low-order modeling of resonance for fixed-valve micropumps based on first principles. J Microelectromech Syst 12:325–334

Muralt P (2000) Ferroelectric thin films for micro-sensors and actuators: a review. J Micromech Microeng 10:136–146

Naik RS, Lutsky JJ, Reif R, Sodini CG (1998) Electromechanical coupling constant extraction of thin-film piezoelectric materials using a bulk acoustic wave resonator. IEEE Trans Ultrason Ferroelectr Freq Control 45:257–263

Nguyen NT, Huang XY, Chuan TK (2002) MEMS-micropumps: a review. J Fluid Eng Trans ASME 124:384–392

Olsson A, Enoksson P, Stemme G, Stemme E (1997) Micromachined flat-walled valveless diffuser pumps. J Microelectromech Syst 6:161–166

Redwood M (1961) Transient performance of a piezoelectric transducer. J Acoust Soc Am 33:527–536

Rodahl M, Kasemo B (1996a) A simple setup to simultaneously measure the resonant frequency and the absolute dissipation factor of a quartz crystal microbalance. Rev Sci Instrum 67:3238–3241

Rodahl M, Kasemo B (1996b) Frequency and dissipation-factor responses to localized liquid deposits on a QCM electrode. Sens Actuator B Chem 37:111–116

Rodahl M, Hook F, Kasemo B (1996) QCM operation in liquids: an explanation of measured variations in frequency and Q factor with liquid conductivity. Anal Chem 68:2219–2227

Setter N, Damjanovic D, Eng L et al (2006) Ferroelectric thin films: review of materials, properties, and applications. J Appl Phys 100:051606

Standards Committee of the IEEE Ultrasonics, Ferroelectrics, and Frequency Control Society (1978) Standard definitions and methods of measurement for piezoelectric vibrators. IEEE ANSI/IEEE Std. 177-1978, New York

Standards Committee of the IEEE Ultrasonics, Ferroelectrics, and Frequency Control Society (1987) IEEE standard on piezoelectricity. IEEE ANSI/IEEE Std. 176-1987, New York

Valimaki H, Lekkala J, Helle H (1997) Prediction ability of a lumped-element equivalent-circuit model for thickness-shear mode resonators in liquids. Sensor Actuator A 60:80–85